

PNNL-11806 UC-602

esi

Pacific Northwest National Laboratory

Operated by Battelle for the U.S. Department of Energy

Examination of the Surface Coatings Removed from K-East Basin Fuel Elements

J. Abrefah

S. C. Marschman

E. D. Jenson

May 1998

DISTRIBUTION OF THIS DOCUMENT IS UNLIMITED MASTER

Prepared for the U.S. Department of Energy under Contract DE-AC06-76RLO 1830

DISCLAIMER

This report was prepared as an account of work sponsored by an agency of the United States Government. Neither the United States Government nor any agency thereof, nor Battelle Memorial Institute, nor any of their employees, makes any warranty, express or implied, or assumes any legal liability or responsibility for the accuracy, completeness, or usefulness of any information, apparatus, product, or process disclosed, or represents that its use would not infringe privately owned rights. Reference herein to any specific commercial product, process, or service by trade name, trademark, manufacturer, or otherwise does not necessarily constitute or imply its endorsement, recommendation, or favoring by the United States Government or any agency thereof, or Battelle Memorial Institute. The views and opinions of authors expressed herein do not necessarily state or reflect those of the United States Government or any agency thereof.

> PACIFIC NORTHWEST NATIONAL LABORATORY operated by **BATTELLE** for the UNITED STATES DEPARTMENT OF ENERGY under Contract DE-AC06-76RLO 1830

> > Printed in the United States of America

Available to DOE and DOE contractors from the Office of Scientific and Technical Information, P.O. Box 62, Oak Ridge, TN 37831; prices available from (615) 576-8401.

Available to the public from the National Technical Information Service, U.S. Department of Commerce, 5285 Port Royal Rd., Springfield, VA 22161

DISCLAIMER

Portions of this document may be illegible in electronic image products. Images are produced from the best available original document.

Examination of the Surface Coatings Removed from K-East Basin Fuel Elements

- J. Abrefah
- S. C. Marschman
- E. D. Jenson

May 1998

Prepared for the U.S. Department of Energy under Contract DE-AC06-76RLO 1830

Pacific Northwest National Laboratory Richland, Washington 99352

				•
		•		
i		· ·		•
			•	•

Summary

This report provides the results of studies conducted on coatings discovered on the surfaces of some N-Reactor spent nuclear fuel (SNF) elements stored at the Hanford K-East Basin. These elements had been removed from the canisters and visually examined in-basin during FY 1996 as part of a series of characterization tests. The characterization tests are being performed to support the Integrated Process Strategy developed to package, dry, transport, and store the SNF in an interim storage facility on the Hanford Site.

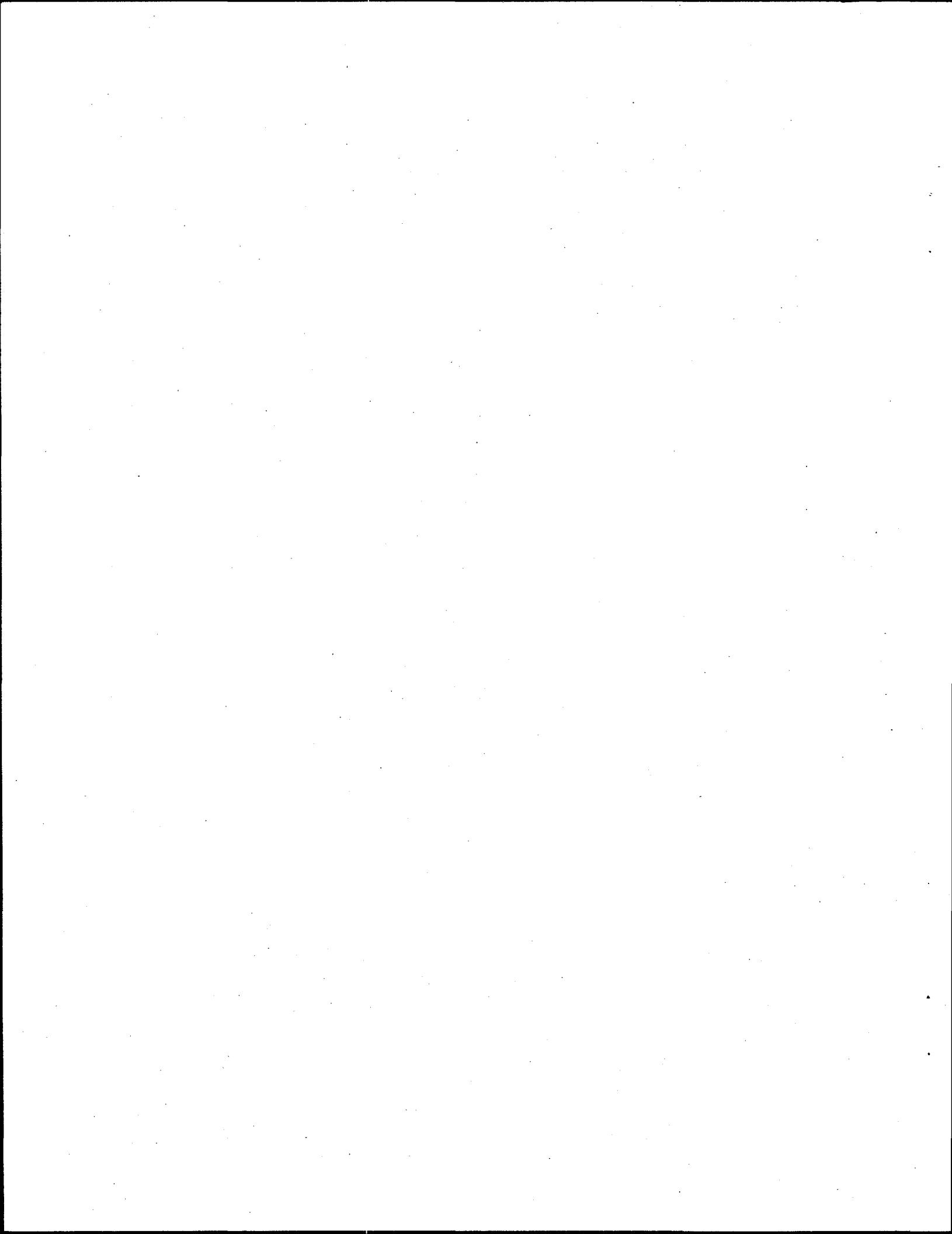
Samples of coating materials were removed from K-East canister elements 2350E and 2540E, which had been sent, along with nine other elements, to the Postirradiation Testing Laboratory (327 Building) for further characterization following the in-basin examinations. These coating samples were evaluated by Pacific Northwest National Laboratory using various analytical methods. This report is part of the overall studies to determine the drying behavior of corrosion products associated with the K-Basin fuel elements.

Altogether, five samples of coating materials were analyzed. These samples were identified by X-ray diffraction analysis to primarily be composed of uranium oxides and oxyhydrates. Scanning electron microscope analysis showed these samples to consist of small needles or agglomerates composed of smaller particulates and needles. This composition indicates the coatings may be formed as part of a nucleation and precipitation process. Thermogravimetric analysis combined with the total weight of material recovered from some of the elements yielded a water-content-per-surface-area-of-fuel estimate of 6·10-6 mol water/cm². These analyses suggest that hydration of the coating materials could be an additional source of moisture in the Multi-Canister Overpacks being used to contain the fuel for storage.

•
•
·
·.
·
٠
•
٠

Acknowledgment

The authors extend their appreciation to Mr. H. Craig Buchanan for his support of the thermogravimetric analyses.



Quality Assurance

This work was conducted under the Quality Assurance Program, Pacific Northwest National Laboratory (PNNL) SNF-70-001, SNF Quality Assurance Program, as implemented by the PNNL SNF Characterization Project Operations Manual. This QA program has been evaluated and determined to effectively implement the requirements of DOE/RW-0333P, Office of Civilian Radioactive Waste Management, Quality Assurance Requirements and Description (QARD). Compliance with the QARD requirements is mandatory for projects which generate data used to support the development of a permanent High-Level Nuclear Waste repository. Further, the U.S. Department of Energy has determined that the testing activities which generated the results documented in this report shall comply with the QARD. Supporting records for the data in this report are located in the permanent PNNL SNF Characterization Project records, Examination of the Surface Coatings Removed from K-East Basin Fuel Elements.

4 · *					
	•				
		•			
•					
•					
			٠.		
•					
			•		
			•		
					•
		•			
	•				
•	•				
•					
				•	
•					
		•			
				*	
					•
				•	
					•
					*
				•	•
,					
,					

Contents

Sun	nmary	iii
Ack	nowledgment	v
Qua	lity Assurance	vii
Acr	onyms	xi
1.0	Introduction	1.1
2.0	X-ray Diffraction Analysis	2.1
3.0	Scanning Electron Microscopy Examination	3.1
4.0	Drying Characteristics of the Surface Coating	4.1
	4.1 Drying of Coating Material	4.1
	4.2 Drying Mechanism	4.4
5.0	Water Content of Coating Samples	5.1
6.0	Conclusions	6.1
7.0	References	7.1

Figures

2.1	Macrophotograph of End Region of Fuel Element from Canister 2350E	2.2
2.2	Macrophotograph of End Region of Fuel Element from Canister 2540E	2.3
2.3	Background Substracted X-ray Spectrum and "Stick Figure" Patterns of Phases Identified for Coating Sample SFEC20, 2350E-SD3	2.5
3.1	Scanning Electron Micrograph of Coating Materials Removed from the Surface of an N-Reactor Outer Fuel Element Stored in the K-East Basin Canister 2350E. There are some needle-type precipitates present in this view, but there is a higher percentage of larger agglomerates comprising either small needles or round particulates	3.2
3.2	Scanning Electron Micrograph of Coating Materials Removed from the Surface of an N-Reactor Outer Fuel Element Stored in the K-East Basin Canister 2350E. This view shows the needle-type precipitates prevalent on the surface of the fuel element	3.3
4.1	Weight Loss, Temperature, and MS Signal for Water Versus Time for Element 2350E Surface Coating for (a) First 5 Segments and (b) Last 4 Segments	4.3
4.2	Combined Weight Loss and Temperature History Versus Time for Element 2350E Surface Coating	4.4
	Tables	
2.1	XRD Analyses of Coating Materials Recovered from the Surface of Two N-Reactor Fuel Elements Stored in the K-East Basin	2.4
4.1	Weights of Coating Samples	4.1

Acronymns

DSC differential scanning calorimeter

MCOs Multi-Canister Overpacks

MS mass spectrometer

QA Quality Assurance

QARD Quality Assurance Requirements and Description

SEM scanning electron microscope

SNF spent nuclear fuel

TGA thermogravimetric analysis

XRD X-ray diffraction

1.0 Introduction

Characterization studies conducted in FY 1996 on Hanford N-Reactor spent nuclear fuel (SNF) included in-basin visual examinations of fuel elements removed from K-East Basin canisters. During the examinations, many of these elements appeared to be light-gray, except on the ends that were sitting in sludge, which appeared black. The examination campaign also noted that many fuel elements had small regions of other colors on the surface. Some of these other colors may be attributed to rust (iron oxyhydrates) or uranium oxyhydrates.

Initially, gray was thought to be the "true" color of the fuel. However, a subsequent fuel washing demonstration project (Maassen 1997) subjected several elements to an aggressive cleaning. One of the cleaning methods used ring-shaped wire brushes to scrub the fuel element surfaces. The brushes removed the gray color, revealing the actual surface of the fuel, which appeared dark-gray-to-black in nature. This dark base color is consistent with the color of the surfaces of as-fabricated fuel. Thus, the gray material appeared to be a type of film coating on the fuel surface, but its formation process has not yet been determined.

Following the in-basin examinations (Pitner 1997), 11 fuel elements were selected for further characterization testing and sent to the Postirradiation Testing Laboratory (327 Building). All 11 elements were visually examined (videotaping of entire exposed surfaces and macrophotography), and the gray coating observed. Because this surface coating was not anticipated, some of the material was recovered for analysis by Pacific Northwest National Laboratory^(a) to gain insight on its possible effects on SNF during dry storage. Two outer elements (removed from K-East canisters 2350E and 2540E) were selected for destructive examination, and samples of the gray coating were recovered from these elements. The studies on these coating samples are discussed in this report.

The samples were analyzed by X-ray diffraction (XRD) to identify phases and phase compositions. These results were used to develop an estimate of water content of the coatings as a function of unit fuel surface area. Portions of the collected coatings were examined using a scanning electron microscope (SEM). The SEM was used to determine coating material morphology. Finally, some of these samples were analyzed using thermogravimetric analysis coupled with mass spectrometry (TGA/DSC/MS/system) to determine the drying characteristics. The results of these analyses are given here.

⁽a) Operated by Battelle for the U.S. Department of Energy under Contract DE-AC06-76RLO 1830.

2.0 X-ray Diffraction Analysis

Five coating samples from the two fuel elements were collected by scraping the surfaces with simple tools or burnishing them with small pieces of abrasive pads. The five samples were sent to the Radiochemical Processing Laboratory (325 Building hot cells) for further examination by XRD followed by SEM examinations. The SEM was coupled with an energy dispersive for X-ray analyzer to better determine particulate size and elemental analysis of the material. Four samples were taken from the (predominantly) gray coating areas of the two elements, while one was taken (on a best-effort basis) from an area that appeared to be reddish.

Figures 2.1 and 2.2 show macrophotographs of the end regions that sat on the bottom of the canisters. The gray coating is apparent, as are the dark end areas that had been immersed in sludge. The reddish-colored regions can only be identified on the element taken from canister 2350E, and are highlighted by the dotted lines. The photos of the element taken from canister 2540E were developed in black and white; the reddish-colored regions cannot be identified from the photos (although no problems were encountered for sample recovery as the regions could clearly be seen through the yellow-tinted hot cell windows).

The gray coating was easily scraped, scored, or marred. This is noted on the photographs where the process of conducting the photographic examinations caused scoring on the surface of the element. The process of rotating the element on the support stand rollers left a clear mark on the gray coating.

The XRD samples were prepared in the Shielded Analytical Laboratory located within the 325 Building, followed by analysis using the Lab 409 XRD. The phases identified for each sample are shown in Table 2.1. Note that some of the different crystallographic phases identified have the same phase composition.

The XRD results were analyzed for the presence of silicon-, aluminum-, calcium-, iron-, and uranium-based oxides and oxyhydrates. Only uranium-based constituents were identified by XRD. An XRD spectrum for coating sample 2350E-SD3 is shown in Figure 2.3. All the major peaks were identified. The broadening of some of the peaks may be due to noncrystalline fractions of the sample. It is interesting to note the range of uranium oxides and oxyhydrates that were identified in the coatings. The presence of oxides and hydrates suggests a complex range of thermochemical reactions have occurred, and the possibility of radiolytically enhanced reactions aiding the formation of some of these compounds cannot be dismissed. Regardless of how these compounds are formed, the decomposition properties of the oxyhydrates are interesting with respect to understanding some of the TGA drying curves being measured for fuel and sludge. These properties will also be important in evaluating their impact from the standpoint of residual water that may end up in the Multi-Canister Overpacks (MCOs) being used to contain the SNF for interim dry storage.

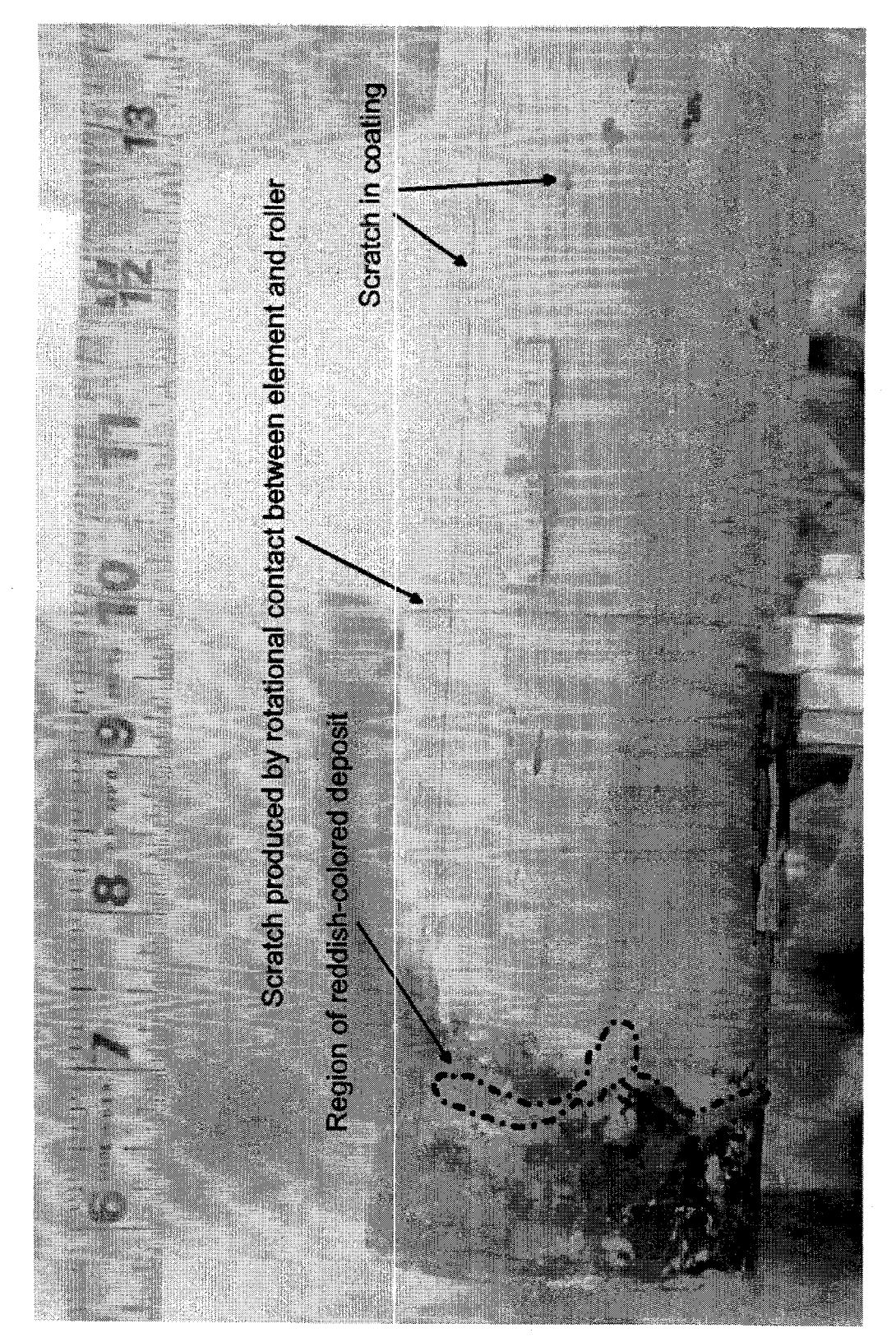


Figure 2.1. Macrophotograph of End Region of Fuel Element from Canister 2350E

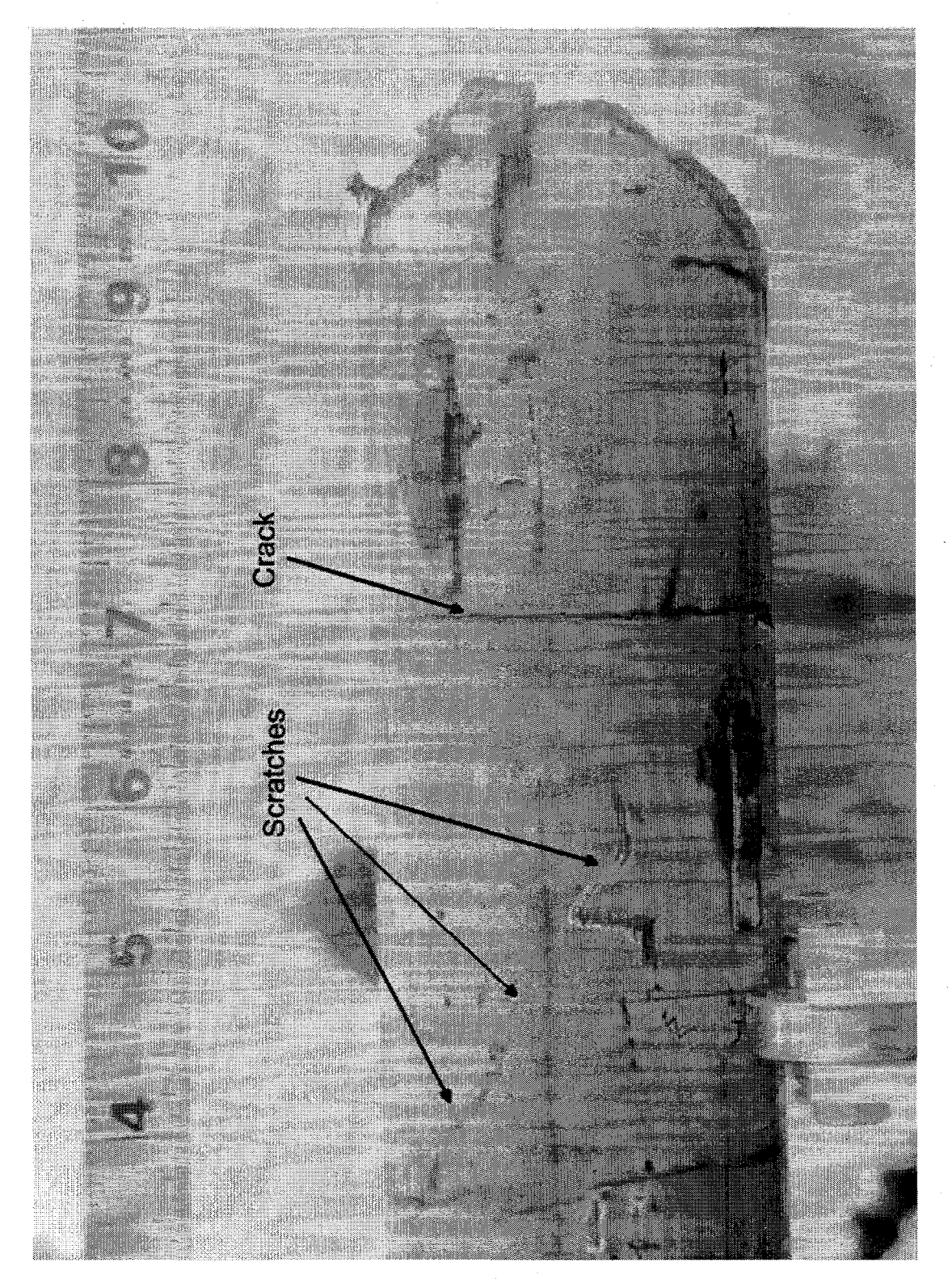


Figure 2.2. Macrophotograph of End Region of Fuel Element from Canister 2540E

Table 2.1. XRD Analyses of Coating Materials Recovered from the Surface of Two N-Reactor Fuel Elements Stored in the K-East Basin

		Phase
Sample Number	Phases Identified	Composition
SFEC20,2350E-SD1	Uranium Oxide Hydrate	UO ₄ ·2H ₂ O
(sample of the reddish-colored material)	Metastudtite	UO₄·2H₂O
	Uranium Oxide	U_3O_8
SFEC20,2350E-SD2	Studtite	UO ₄ ·4H ₂ O
(small sample carefully scraped from the	Metastudtite	UO₄·2H₂O
surface to avoid cross-contamination with	Uranium Oxide	UO ₃
other materials)	Uranium Oxide Hydrate	UO₄·2H₂O
SFEC20,2350E-SD3	Studtite	UO₄·4H₂O
(bulk sample taken using abrasive pad)	Uranium Oxide	UO ₃
	Uranium Oxide Hydrate	UO₄·2H₂O
SFEC04,2540E-SD1	Studtite	UO ₄ ·4H ₂ O
(small sample carefully scraped from the	Uraninite-Q, syn	U ₃ O ₇
surface to avoid cross-contamination with	Uraninite-syn	UO ₂
other materials)	Uraninite-syn	U ₄ O ₉
	Uranium Oxide	U_3O_7
	· Paraschoepite	UO _{2.86} ·1.5H ₂ O
SFEC04,2540E-SD2	Studtite	UO ₄ ·4H ₂ O
(bulk sample taken using abrasive pad)	Uraninite-Q, syn	U_3O_7
	Uraninite-syn	UO ₂
	Uraninite-syn	U ₄ O ₉
	Uranium Oxide	U_3O_8
	Uranium Oxide	UO ₃
:	Paraschoepite	UO _{2.86} ·1.5H ₂ O

The most complex uranium oxyhydrates found during this analysis include $UO_4\cdot 4H_2O$ and $UO_{2.86}\cdot 1.5H_2O$. The presence of a UO_4 -based hydrate, found in easily measurable quantities on the fuel, is interesting, as these types of hydrates historically have been difficult to fabricate in the laboratory. On the other hand, it is much easier to predict and understand the presence of the UO_3 -based hydrates because they have been the subject of numerous studies.

For both families of hydrates, dehydration information dates back to the 1800s. The dehydration process for UO₄·4H₂O has been studied by many researchers, including Huttig and Schroeder (1922), Cordfunke (1961), Cordfunke and van der Gieesen (1963), and Sato (1963). These studies are consistent in presenting information on the first dehydration reaction (as measured in air atmospheres).

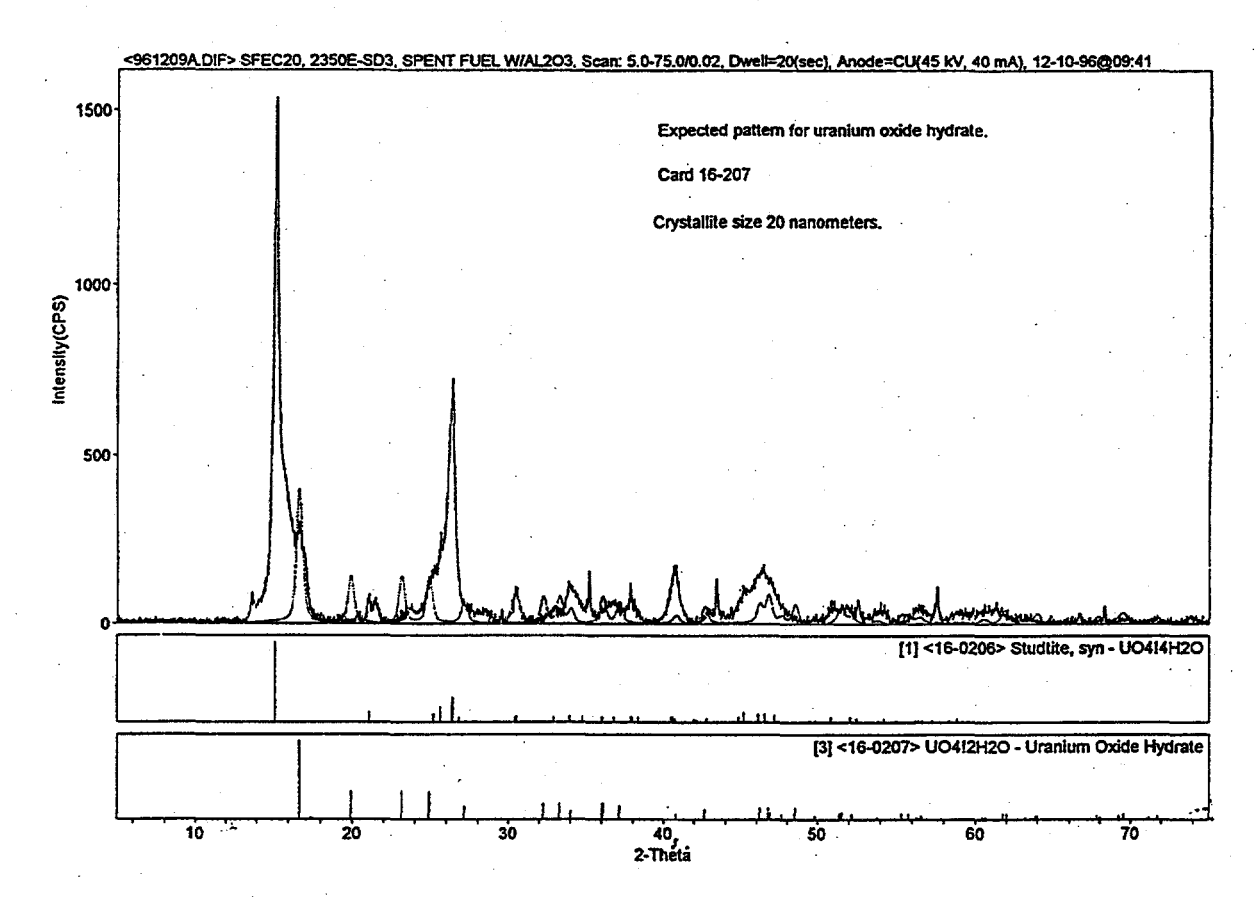


Figure 2.3. Background Substracted X-ray Spectrum and "Stick Figure" Patterns of Phases Identified for Coating Sample SFEC20, 2350E-SD3

The first reaction may be summarized as:

$$UO_4\cdot 4H_2O \rightarrow UO_4\cdot 2H_2O$$

 $\sim 60^{\circ}C < T < \sim 100^{\circ}C$

A reaction in this temperature range was observed during TGA studies being conducted on fuel materials.

The dehydration of UO₄·2H₂O occurs by the thermal decomposition reaction:

$$UO_4 \cdot 2H_2O \rightarrow UO_3$$
 (X-ray amorphous or α -phase)
~420°C < T < ~550°C

Evidence of this reaction is also present in data obtained from TGA drying studies (Section 4.2). There are data in the early literature (referenced in Katz and Rabinowitch 1951) that suggest the dehydration of UO₄ hydrates may break down to form UO₃-based hydrates [and indeed, these UO₄ hydrates have been identified in the gray film samples examined by XRD in the present study]. However, these reactions are

not supported by later studies (conducted since 1960). A more plausible explanation for the presence of UO_3 -based hydrates lies in their direct formation from uranium oxides rather than decomposition of UO_4 - $2H_2O$.

The formation of UO₃ from UO₃-based hydrates was reported by Wheeler et al. (1964), who performed an extensive review of the (then-current) literature and documented three forms: UO₃·2H₂O, UO₃·H₂O, and UO₃·0.5H₂O. In the present study, the mineral phase, "paraschoepite," was identified, with a corresponding composition identified as UO_{2.86}·1.5H₂O. Wheeler et al. acknowledged the possibility that modified forms of "schoepite" (UO₃·2H₂O) could exist but dismissed the evidence in the literature of the time as speculative. However, the existence of these modified species has since been determined.

Wheeler et al. (1964) also reported information on the decomposition of the hydrates. They did not report details of the reaction mechanisms because they simply prepared mixtures of various hydrates to determine what phases of oxide would be formed by thermal decomposition. The decomposition process was performed using differential thermal analysis. The authors note the following reaction:

$$UO_3 \cdot 2H_2O \rightarrow UO_3 \cdot H_2O$$

~100°C < T < ~160°C

The decomposition of UO₃·H₂O then follows at higher temperatures:

$$UO_3 \cdot H_2O \rightarrow UO_3$$

~360°C < T < ~400°C

The decomposition of $UO_3 \cdot H_2O$ can also decompose to $UO_3 \cdot 0.5H_2O$. The decomposition reaction of $UO_3 \cdot 0.5H_2O$ is represented as:

$$UO_3 \cdot 0.5H_2O \rightarrow UO_3$$

~500°C < T < ~550°C

This last decomposition reaction is of particular interest for comparison to the TGA studies performed on K-Basin fuel and on sludge (Abrefah et al. 1998). The decomposition of the UO₃ hemi-hydrate may be a possible explanation.

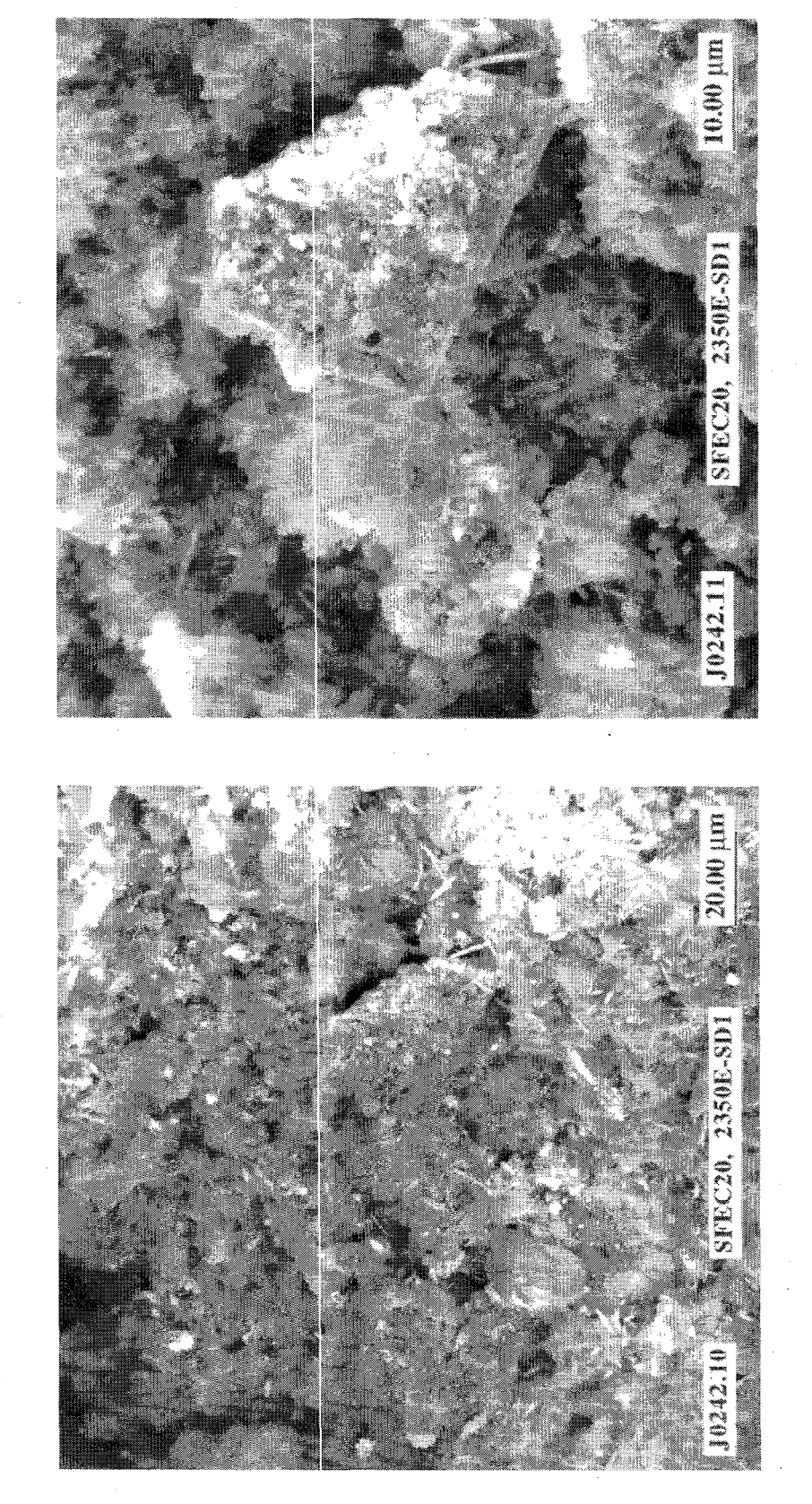
From this limited analysis of the literature data, it appears that thermal treatment may be possible for the removal of water from hydrated species. However, some water may remain due to the presence of hydrates such as UO₃·0.5H₂O, which will not release water at lower temperatures. Furthermore, the limited literature review did not provide enough information to determine all of the possible reactions that may occur between the various oxides and hydrates detected by XRD, and some high-temperature species may have been missed.

3.0 Scanning Electron Microscopy Examination

Scanning electron microscopy was used to determine the particulate morphology of the coating samples. The particulates appeared in two general classifications: 1) agglomerates of smaller particles and 2) needle-shaped particles found individually or in agglomerates of larger particles.

Figures 3.1 and 3.2 show the two different types of particulates. Both of the samples shown were taken from the gray coating that predominated the surface of element 2350E. In Figure 3.1, the particle size in the agglomerates appears to be submicron. The agglomerates themselves range in size from a few microns to about 30 μ m. These agglomerates also appear to have needle-shaped particles incorporated into their matrix. Figure 3.2 shows a view of an area composed primarily of needle-shaped particles. There is evidence that some of the particles may be plate-like in morphology. The needles appear to range from a few microns to about 20 μ m in length and from 1 μ m to about 5 μ m in width.

The presence of needle-shaped particles suggests that the coating material is composed of precipitation products resulting from fuel corrosion. Needle-shaped precipitates are often observed as the result of heterogeneous nucleation followed by growth in a liquid medium (1,10-phenanthrolene precipitated from a saturated water solution is a classic example). Because these precipitates consist of uranium oxyhydrates, it can be postulated that the water environment surrounding the fuel surfaces is saturated with uranium (a concentration level of about 4 ppm). Two possible explanations are: 1) the uranium fuel corrosion rate could have been high enough to supersaturate the water surrounding the fuel, and precipitation occurred before the water could be processed by the ion exchange filters; 2) there could be poor circulation within the basins, particularly inside the fuel storage canisters. The fuel corrosion could have proceeded at any rate, but, over time, supersaturation is reached and the dissolved uranium precipitates as the oxyhydrate. This scenario would suggest that the water surrounding the fuel elements has a different level of dissolved species than that found in the bulk of the K-East Basin water. This could explain, for example, why the cesium content found in the ion exchange filters may not be representative of the corrosion rate of the fuel in the basin.



Scanning Electron Micrograph of Coating Materials Removed from the Surface of an N-Reactor Outer Fuel Element Stored in the K-East Basin Canister 2350E. There are some needle-type precipitates present in this view, but there is a higher percentage of larger agglomerates comprising either small needles or round particulates. Figure 3.1.

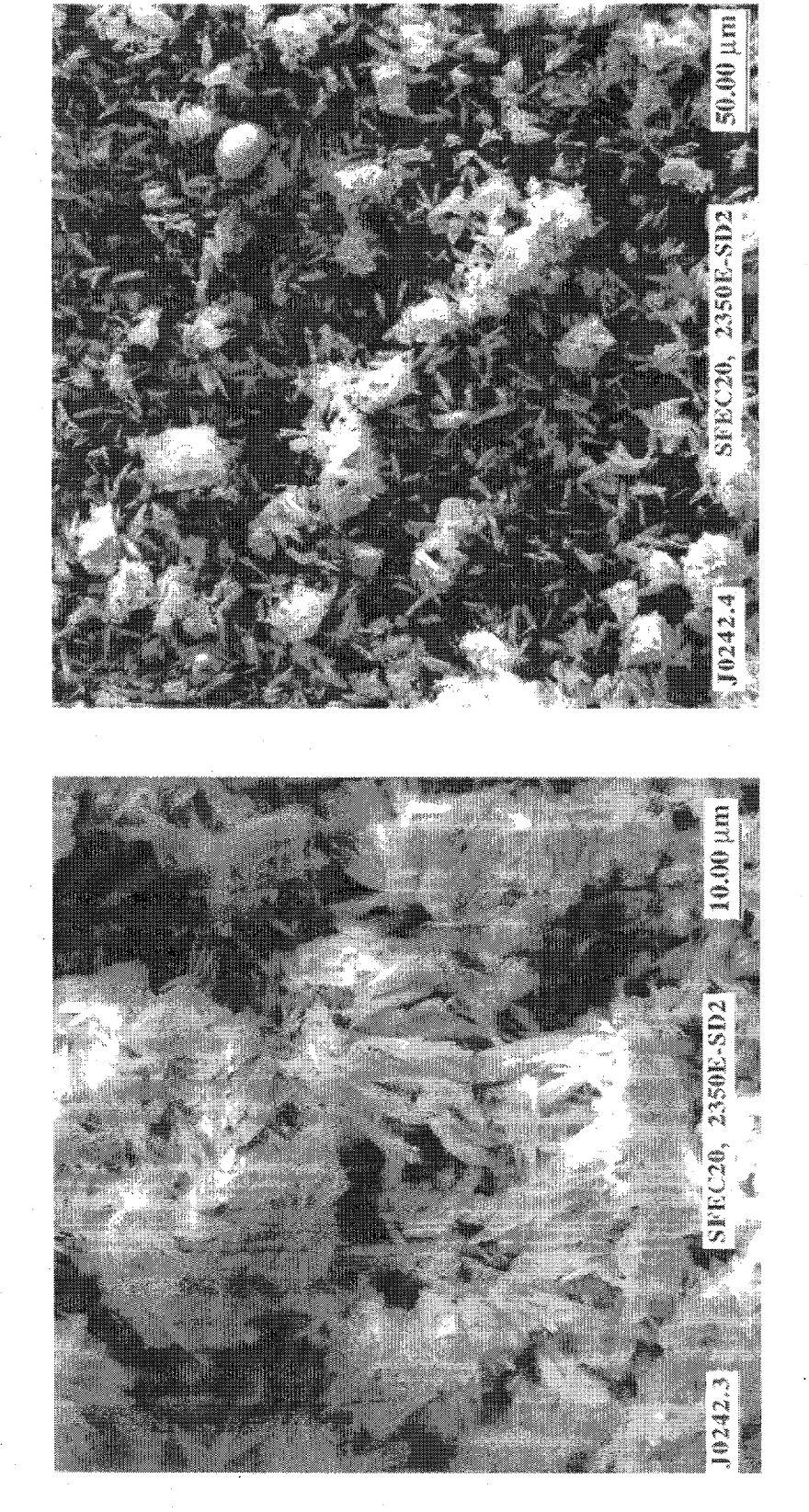


Figure 3.2. Scanning Electron Micrograph of Coating Materials Removed from the Surface of an N-Reactor Outer Fuel Element Stored in the K-East Basin Canister 2350E. This view shows the needle-type precipitates prevalent on the surface of the fuel element.

4.0 Drying Characteristics of the Surface Coating

Two of the five coating samples collected from the SNF elements had enough material for drying studies using the TGA/DSC/MS system (thermogravimetric analysis/differential scanning calorimeter/mass spectrometer) (Netzsch STA 409). A brief discussion of the system is given in Abrefah et al. (1998). The two drying tests performed used about 57 mg of coating material from SNF element 2540E and about 209 mg of coating material from SNF element 2350E.

4.1 Drying of Coating Material

The sample material, contained in an alumina crucible, was subjected to the following heating cycles in a vacuum of about 10⁻³ Torr:

- heated at a constant rate of 0.5°C/min to a temperature of about 50°C and held at this temperature for 10 hours
- heated at a constant rate of 0.5°C/min to a temperature of about 75°C and held at this temperature for 10 hours
- heated at a constant rate of 1°C/min to a temperature of about 300°C and held at this temperature for 10 hours
- heated at a constant rate of 1°C/min to a temperature of about 850°C and held at this temperature for 2 hours, followed by a cooling down to ambient condition.

The electrobalance monitored the changes in the sample weight, and the attached quadrupole mass spectrometer was used to monitor most of the expected gaseous species, for example, water and its cracking ions, and volatile fission products, such as iodine and krypton.

The before and after drying test weight measurements of the coating samples are listed in Table 4.1. The two coatings lost weight due to thermal decomposition of the hydrates. Both samples lost about 23 wt% of their initial weight (last column of Table 4.1). The same percent weight loss by the two samples suggests a probable similar chemical phase and water content.

Table 4.1. Weights of Coating Samples

	Sample Sample Weight (mg)		Percent Weight	
TGA Run	Identification	Before Test	After Test	Loss
34	04-SD2	57	44	23
35	20-SD3	209	161	23

The TGA weight change and MS data for Run 34 were very noisy and are not be reported here, but the data for Run 35 are plotted in Figures 4.1 and 4.2. The system experienced an electrical power failure during Run 35. Shown in Figure 4.1a is the weight loss and the MS signal for H_2O^+ for the run before the power interruption. This part of the test covered the first five temperature segments of the run:

- 1. ramp from ambient temperature to 50°C
- 2. held at 50°C for 10 hours
- 3. ramp from 50°C to 100°C
- 4. held at 100°C for 10 hours
- 5. ramp from 100°C to 300°C.

Figure 4.1a indicates a relatively small weight loss by the sample at 50°C followed by a substantial weight loss for the temperature segments 3 and 4. The weight loss seems to have stabilized during the hold at 100°C, but the sample started losing weight again during the ramp from 100°C to 300°C. The sample experienced about half of the total weight loss between ambient temperature and the hold at 100°C.

Figure 4.1b shows the continuation of the weight loss by the sample after the power interruption. The weight loss in Figure 4.1b can be categorized into two portions. The first portion is the weight loss that started during the ramp from 100°C to 300°C. This segment of the sample weight loss seemed to have stabilized during the hold temperature of 300°C. The second portion of weight loss started when the sample temperature reached about 420°C, and the tail end of the data suggests this segment of weight loss was not completed at the end of the run.

The combined weight loss (i.e., Figures 4.1a and 4.1b) of the coating sample and the test temperature history are shown in Figure 4.2. Figure 4.2 shows that the coating sample lost a total of about 40 mg, which compares reasonably with the before and after test weight loss of about 48 mg. Two factors could influence the two measurements. Handling difficulties of the sample to and from the hot cell where the weights were measured may have caused loss of material and, consequently, caused a higher weight loss measurement. The power interruption during the test made it difficult to determine exact weight change of the sample. These two factors, together with other experimental inaccuracies, may have accounted for the observed differences in the two weight loss measurements. For the total weight loss measured by the TGA during the test, about 18 mg occurred between ambient temperature and 100°C (including the hold at 100°C), and the remaining occurred at temperatures above 100°C.

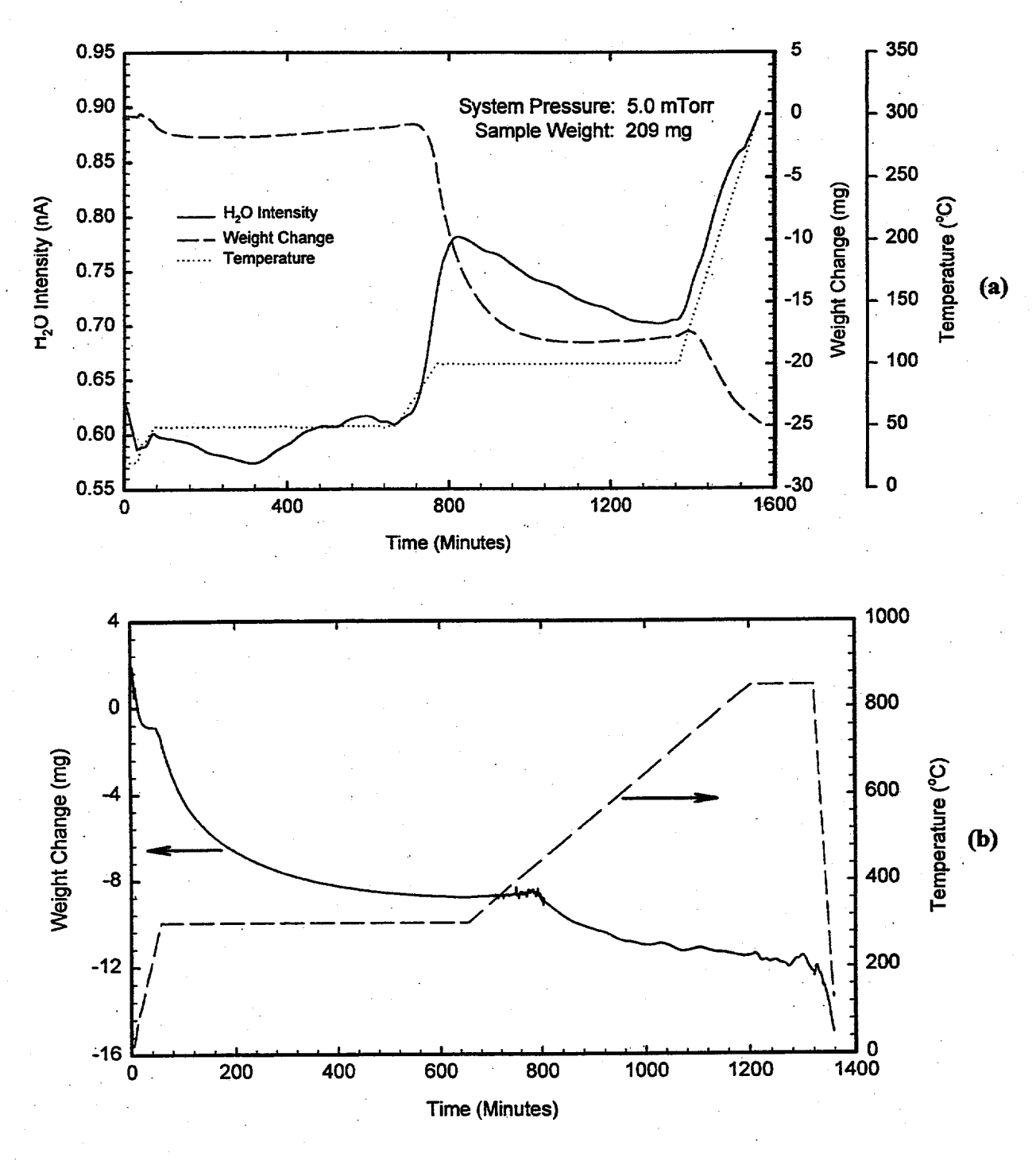


Figure 4.1. Weight Loss, Temperature, and MS Signal for Water Versus Time for Element 2350E Surface Coating for (a) First 5 Segments and (b) Last 4 Segments

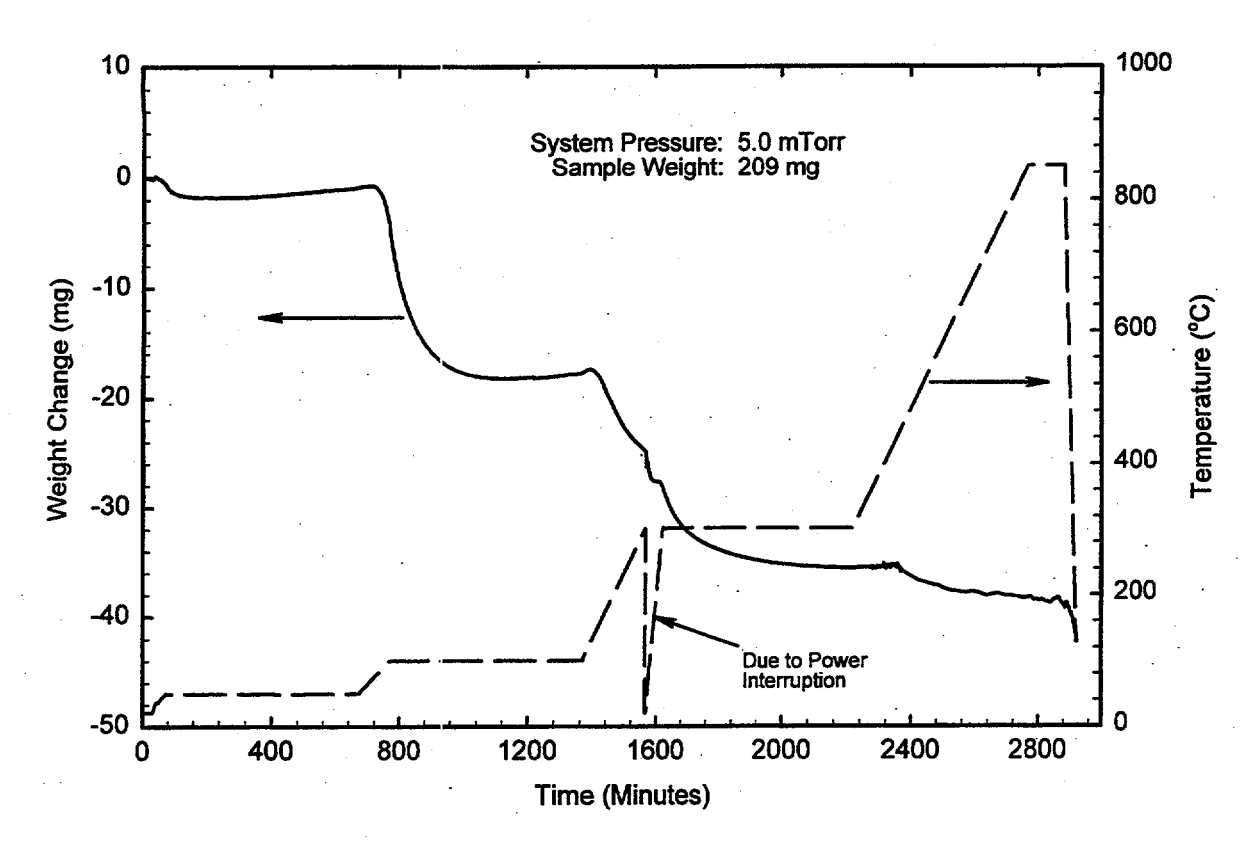


Figure 4.2. Combined Weight Loss and Temperature History Versus Time for Element 2350E Surface Coating. The temperature curve shows where the power failure occurred during the run.

4.2 Drying Mechanism

The XRD spectrum of the coating sample from element 2350E indicates that the uranium peroxide hydrate, UO₄·4H₂O, is the main hydrated phase in the coating. As discussed in Section 2.0, the thermal decomposition of UO₄·4H₂O has been studied by other researchers, including Huttig and Schroeder (1922), Cordfunke (1961), and Cordfunke and van der Giessen (1963), who reported a two-step decomposition reaction:

1. Decomposition of UO₄·4H₂O to UO₄·2H₂O

$$UO_4: 4H_2O \rightarrow UO_4: 2H_2O + 2H_2O$$
 (4.1)

2. Decomposition of UO₄·2H₂O to UO₃

$$UO_4 \cdot 2H_2O \rightarrow UO_3 + 2H_2O + \frac{1}{2}O_2$$
 (4.2)

Comparison of these reaction steps with the observed weight loss measurements of the coating suggests that the weight loss between the ambient temperature and 100°C may be due to the first

decomposition reaction step (i.e., Equation 4.1). This inference is supported by the observed weight loss of about 9 wt% (18 mg), which agrees well with a theoretical estimate of about 10 wt%. Additionally, the results indicated the decomposition temperature range of the UO₄·4H₂O phase to the UO₄·2H₂O to be about 50°C to 100°C, the same temperature range reported by Sato (1963) and Cordfunke and van der Giessen (1963).

The thermal decomposition of the dihydrate, $UO_4 \cdot 2H_2O$ (Equation 4.2), was concluded to be the cause of the measured weight loss by the coating within the temperature range of >100°C up to 400°C. The last segment of the weight loss data (i.e., above 400°C) may be due to any combination of the following factors:

- 1. thermal decomposition of other hydroxides (e.g., hydroxides of uranium, iron and aluminum oxides)
- 2. reduction reaction of UO₃ to U₃O₈
- 3. continuation of the incomplete reaction of the dihydrate decomposition at higher temperatures.

The XRD examination of the coating sample (Table 2.1 and Figure 2.3) failed to identify any of the hydroxides of (1). The negative results for these chemical phases suggested that their contribution to the observed weight loss of the coating samples was small. The reduction reaction in (2) has been reported by Cordfunke and van der Giessen (1963) to have occurred at temperatures above 425°C. For the present coating sample test, the weight loss that can be conclusively ascribed to the dihydrate decomposition constitutes about 8 wt% of the initial sample weight. The theoretical prediction of Equation (4.2) is about 14 wt%, which compares reasonably within experimental errors with the measured data but indicates that the decomposition process was not completed. Adding the last segment weight loss of about 2.4 wt% to the value identified as due to the dihydrate decomposition (i.e., 8 wt%) gives a total of about 10.4 wt%, which then agrees with the theoretical estimate, given that the sample was not pure tetrahydrate. The preceding discussions suggest that (2) and (3) may be the main factors affecting the weight loss measured at temperatures above 400°C.

5.0 Water Content of Coating Samples

The total weight of material present on the surfaces could not be determined with a high degree of accuracy because 1) some of the material was lost during brushing; 2) the brushing cannot be guaranteed to be complete because it may not have removed all coating materials; and 3) some of the sample remained in the abrasive pad, which was not weighed prior to use.

The majority of the coating material recovered from the surfaces of these two elements was analyzed using TGA/DSC/MS (discussed in Section 4.0). Each sample used for TGA weighed approximately 200 mg. The very light weight of the material was unexpected based on literature references for the densities of UO₄·4H₂O and UO₄·2H₂O and the amount of volume occupied by the samples in the TGA crucibles. Similar volumes of K-East canister sludge have weighed about 1.5 grams. The SEM images of the coatings indicate that these materials are primarily flocculant agglomerates of submicron particles.

Because the thickness of these coatings cannot be easily determined, a theoretical density cannot be calculated. However, the amount of material per unit area of fuel surface can be estimated. Coupled with the XRD compositional information, the amount of water per unit surface area of fuel can be estimated. A factor of 3 was multiplied to the mass of particulate recovered to account for, and likely overestimate, the material lost or contained in the brush material.

Driver fuel element dimensions were used to calculate the surface area of the outer fuel elements taken from K-East canister 2350E. As measured from a composite series of macrophotographs, the tube-shaped N-Reactor element has the following dimensions:

~22 inches long	2.347 inches	0.495 inches thick	~170 in.2 surface
(~56 cm)	outer diameter	(~1.25 cm)	area cleaned
	(~6 cm)		$(\sim 1095 \text{ cm}^2)$

Applying the factor of 3 to the mass recovered yields 600 mg of material "coating" a surface area of \sim 1095 cm². The assumption that the coating is found evenly applied across the surface yields a 0.55 mg/cm² fuel surface.

Data from the TGA/DSC/MS analysis suggest that this material is primarily UO₄·4H₂O. The molecular weight of this phase is 374 g/mol. There are 72 grams water/mol of hydrate. Thus, the quantity of water found on the surface of the fuel elements has been estimated to be:

$$\frac{0.55 \text{ mg/cm}^2 \cdot 72 \text{ g water/mol hydrate}}{374 \text{ g/mol hydrate} \cdot 1000 \text{ mg/g} \cdot 18 \text{ g/mol water}} \approx 6 \cdot 10^{-6} \frac{\text{mol water}}{\text{cm}^2 \text{ fuel surface area}}$$

6.0 Conclusions

The results of the analysis performed on the surface coatings samples are summarized below:

- The before and after test weight measurements indicate that the coating samples for the two tests were close to a pure form of uranium peroxide hydrate.
- The decomposition of the tetrahydrate occurs in two reaction steps: 1) decomposition of the tetrahydrate to the dihydrate and 2) decomposition of the dihydrate to UO₃.
- The thermal decomposition of the coating sample tetrahydrate phase occurred on heating between 50°C and 100°C, corresponding to a loss of two molecules of water from the tetrahydrate.
- The thermal decomposition of the dihydrate starts at temperatures above 100°C and may not be completed until about 400°C. At higher temperatures (above 420°C), the reduction reaction of UO₃ to U₃O₈ may be observed.
- The estimate of the water content in the coating yielded about 6 x 10⁻⁶ mol of water/cm².
- The hydration of the coating materials is an indication of an additional source of moisture in the MCOs that will influence the pressurization issue.

7.0 References

Abrefah, J., H. C. Buchanan, and S. C. Marschman. 1998. *Drying Behavior of K-East Canister Sludge*. PNNL-11628, Pacific Northwest National Laboratory, Richland, Washington.

Cordfunke, E. H. P. 1961. "Alpha-UO₃: Its Preparation and Thermal Stability." *J. Inorg. Nucl. Chemistry* 23:285-286.

Cordfunke, E. H. P., and A. A. van der Giessen. 1963. "Pseudomorphic Decomposition of Uranium Peroxide Into UO₃." J. Inorg. Nucl. Chemistry 25:553-555.

Huttig, G. F. and E. V. Schroeder. 1922. Z. Anorg. Chem. 121:243-253.

Katz, J. J., and E. Rabinowitch. 1951. Chemistry of Uranium, Part 1. National Nuclear Energy Series, VIII-5, McGraw-Hill Publishers, New York.

Maassen, D. P. 1997. Testing of Sludge Coating Adhesiveness on Fuel Elements in 105-K West Basin. HNF-SD-SNF-TRP-020, Duke Engineering & Services Hanford, Inc., Richland, Washington.

Pitner, A. L. 1997. Visual Examinations of K East Fuel Elements. HNF-SD-SNF-TI-045, Duke Engineering & Services Hanford, Inc., Richland, Washington.

Sato, T. 1963. "Preparation of Uranium Peroxide Hydrates." Journal of Applied Chemistry 13:361-365.

Wheeler, V. J., R. M. Dell, and E. Wait. 1964. J. Inorg. Nucl. Chem. 26:1829-1845.

Distribution

No. of Copies

OFFSITE

C. L. Bendixsen
Idaho National Engineering and Environmental Laboratory
P.O. Box 1625
Mail Stop 3135
Idaho Falls, ID 83415

A. W. Conklin
Washington State Department of Health
Airdustrial Park
Building 5, Mail Stop LE-13
Olympia, WA 98504-0095

M. A. Ebner
Idaho National Engineering and
Environmental Laboratory
P.O. Box 1625
Mail Stop 3114
Idaho Falls, ID 83415

A. R. Griffith U.S. Department of Energy, Headquarters 19901 Germantown Rd (EM-65) Germantown, MD 20585-1290

T. J. Hull U.S. Department of Energy, Headquarters 19901 Germantown Road (EH-34) Germantown, MD 20874-1290

M. R. Louthan Savannah River Technology Center Materials Technology Center Aiken, SC 29808 No. of Copies

T. E. Madey Rutgers University Bldg. 3865 136 Freylinghuysen Rd Piscataway, NJ 08854

B. K. Nelson U.S. Department of Energy, Headquarters 19901 Germantown Road (EM-65) Germantown, MD 20874-1290

R. G. Pahl, Jr. Argonne National Laboratory P. O. Box 2528 Idaho Falls, ID 83403

R. S. Rosen Lawrence Livermore National Laboratory 20201 Century Blvd., 1ST Floor Germantown, MD 20874

D. Silver Washington State Department of Ecology P.O. Box 47600 Olympia, WA 98504-7600

T. A. Thornton Framatome Cogema Fuels 1180 Town Center Drive Las Vegas, NV 89134

Copies Copies ONSITE 3 Fluor Daniel Northwest 7 DOE Richland Operations Office L. J. Garvin R3-26 F. F. Huang E6-15 F. F. Huang E6-15 D. Bryson S7-41 G. A. Ritter H0-40 R. M. Hiegel S7-41 7 Numatec Hanford Company C. R. Richins C. R. Richins K8-50 K8-50 E. D. Sellers S7-41 G. P. Chevrier H5-25 J-S. Shuen S7-41 T. Choho R3-86 G. D. Trenchard S7-41 T. Choho R3-86 Hanford Inc. L. R. Flament H0-34 T. A. Flament H5-25 J. D. W. Bergmann X3-79 SGN Eurisys Services Corp S. A. Chastain H0-40 H0-40 D. R. Duncan R3-86 A. L. Pajunen R3-86 L. H. Goldmann R3-86 A. L. Pajunen	No. of			No. of			
DOE Richland Operations Office	<u>Copies</u>			Copies			
DOE Richland Operations Office L. J. Garvin R3-26				_			
F. F. Huang E6-15	ON	SITE		3	Fluor Daniel Northwest		
F. F. Huang E6-15							
D. Bryson S7-41 R. M. Hiegel S7-41 P. G. Loscoe S7-41 7 Numatec Hanford Company S7-41 F. C. R. Richins K8-50 E. D. Sellers S7-41 G. P. Chevrier H5-25 J-S. Shuen S7-41 T. Choho R3-86 G. D. Trenchard S7-41 E. R. Cramer H0-34 T. A. Flament H5-25 J. J. Irwin R3-86 J. J. Irwin R3-86 J. P. Sloughter H5-49 H5-49 R. B. Baker H0-40 D. W. Bergmann X3-79 SGN Eurisys Services Corp S. A. Chastain H0-40 D. R. Duncan R3-86 J. R. Frederickson R3-86 J. R. Frederickson R3-86 J. R. Frederickson R3-86 J. J. Jernberg X3-72 J. C. Devine R3-11 J. Jernberg X3-72 J. C. Devine R3-11 J. A. Lawrence (5) H0-40 R. F. Williams R3-11 J. A. Lawrence (5) H0-40 R. F. Williams R3-11 J. A. Swenson R3-86 J. M. Latkovich K9-44 K9-4	7	DOE Richland Operations Offi	<u>ce</u>		L. J. Garvin	R3-26	
R. M. Hiegel P. G. Loscoe S7-41 G. R. Richins K8-50 E. D. Sellers S7-41 T. Choho R3-86 G. D. Trenchard S7-41 T. Choho R3-86 G. D. Trenchard S7-41 E. R. Cramer H0-34 T. A. Flament H5-25 J. J. Irwin R3-86 Hanford Inc. SGN Eurisys Services Corp S. A. Chastain H0-40 D. W. Bergmann X3-79 S. A. Chastain H0-40 D. R. Duncan R3-86 J. R. Frederickson R3-86 L. H. Goldmann R3-86 L. H. Goldmann R3-86 S. L. Hecht H0-40 J. J. Jernberg X3-72 J. C. Devine R3-11 L. A. Lawrence (5) H0-40 R. F. W. Rasmussen X3-85 A. M. Segrest R3-11 J. A. Swenson R3-11 J. A. Swenson R3-11 J. A. Swenson R3-11 J. A. Swenson R3-86 S. R. Gano K2-12 D. J. Trimble H0-40 W. J. Gray P7-27 J. H. Wicks, Jr. X3-79 B. D. Hanson P7-27 J. H. Wicks, Jr. X3-79 B. D. Hanson P7-27 SNF Project Files D. K. Kreid K7-80 J. M. Latkovich K9-44 S. C. Marschman (10) P7-27 S. M. Oliver P7-22 E. W. Gerber R3-11 T. M. Orlando K8-88					F. F. Huang	E6-15	
P. G. Loscoe \$7-41 7 Numatec Hanford Company C. R. Richins K8-50 H5-25 E. D. Sellers \$7-41 G. P. Chevrier H5-25 J-S. Shuen \$7-41 T. Choho R3-86 G. D. Trenchard \$7-41 E. R. Cramer H0-34 T. A. Flament H5-25 H0-25 H0-34 T. A. Flament H5-25 H1-25 H0-34 T. A. Flament H1-25 B. Baker H0-40 D. W. Bergmann K3-86 L. P. Sloughter H5-49 B. A. Chastain H0-40 H0-40 H0-40 H0-40 H0-40 D. R. Duncan R3-86 A. L. Pajunen R3-86 R3-86 L. H. Goldmann R3-86 A. L. Pajunen R3-86 R3-86 L. H. Goldmann R3-86 A. L. Pajunen R3-86 R3-86 R. F. Williams R3-11 R. F		D. Bryson	S7-41		G. A. Ritter	H0-40	
C. R. Richins K8-50 E. D. Sellers S7-41 F. D. Sellers S7-41 F. Shuen S7-41 F. Choho R3-86 G. D. Trenchard S7-41 F. A. Flament H5-25 T. A. Flament H5-26 T. A. Flament H5-24 T. A. Laving R3-86 T. A. L. Pajunen R3-86 T. A. L. Pajunen R3-86 T. Fechnical Advisory Group T. Fechnical Advisory Group T. Fechnical Advisory Group T. Flament H5-24 T. A. Lawrence (5) H0-40 T.		R. M. Hiegel	S7-41				
E. D. Sellers S7-41 G. P. Chevrier H5-25 J-S. Shuen S7-41 T. Choho R3-86 G. D. Trenchard S7-41 E. R. Cramer H0-34 T. A. Flament H5-25 J. J. Irwin R3-86 Hanford Inc. L. R. Miska R3-86 Hanford Inc. L. R. Miska R3-86 Hanford Inc. L. R. Miska R3-86 J. P. Sloughter H5-49 R. B. Baker H0-40 D. W. Bergmann X3-79 SGN Eurisys Services Corp S. A. Chastain H0-40 D. R. Duncan R3-86 A. L. Pajunen R3-86 J. R. Frederickson R3-86 L. H. Goldmann R3-86 Z Technical Advisory Group S. L. Hecht H0-40 J. J. Jernberg X3-72 J. C. Devine R3-11 L. A. Lawrence (5) H0-40 R. F. Williams R3-11 B. J. Makenas H0-40 R. P. Omberg H0-40 32 Pacific Northwest National Laboratory R. W. Rasmussen X3-85 A. M. Segrest R3-11 J. Abrefah (5) P7-27 J. A. Swenson R3-86 S. R. Gano K2-12 D. J. Trimble H0-40 W. J. Gray P7-27 D. J. Watson X3-79 B. D. Hanson P7-27 J. H. Wicks, Jr. X3-74 G. S. Klinger P7-27 SNF Project Files D. K. Kreid K7-80 J. M. Latkovich K9-44 S. C. Marschman (10) P7-27 B. M. Oliver P7-22 B. W. Gerber P7-21 B. M. Oliver P7-22 B. M. Oliver P7-24		P. G. Loscoe	S7-41	7	Numatec Hanford Company		
J-S. Shuen S7-41 T. Choho R3-86		C. R. Richins	K8-50				
G. D. Trenchard S7-41 E. R. Cramer H0-34 T. A. Flament H5-25 Duke Engineering and Services, Hanford Inc. D. W. Bergmann X3-79 S. A. Chastain H0-40 D. R. Duncan R3-86 J. R. Frederickson R3-86 L. H. Goldmann R3-86 L. H. Goldmann R3-86 S. L. Hecht H0-40 J. J. Jernberg X3-72 J. C. Devine R3-11 L. A. Lawrence (5) H0-40 R. P. Omberg H0-40 R. P. Omberg H0-40 R. P. Omberg H0-40 R. W. Rasmussen X3-85 A. M. Segrest R3-11 J. A. Swenson R3-11 J. A. Swenson R3-86 C. A. Thompson R3-86 S. R. Gano K2-12 D. J. Trimble H0-40 D. J. Watson X3-79 J. H. Wicks, Jr. X3-74 S. Fluor Daniel Hanford Fluor Daniel Hanfo		E. D. Sellers	S7-41		G. P. Chevrier	H5-25	
T. A. Flament H5-25		J-S. Shuen	S7-41		T. Choho	R3-86	
Duke Engineering and Services Hanford Inc. C. R. Miska R3-86 Hanford Inc. H0-40 D. W. Bergmann X3-79 SGN Eurisys Services Corp S. A. Chastain H0-40 D. R. Duncan R3-86 A. L. Pajunen R3-86 J. R. Frederickson R3-86 L. H. Goldmann R3-86 S. L. Hecht H0-40 J. J. Jernberg X3-72 J. C. Devine R3-11 L. A. Lawrence (5) H0-40 R. F. Williams R3-11 B. J. Makenas H0-40 R. P. Omberg H0-40 32 Pacific Northwest National Laboratory R. W. Rasmussen X3-85 A. M. Segrest R3-11 J. Abrefah (5) P7-27 J. A. Swenson R3-11 J. P. Cowin K8-88 C. A. Thompson R3-86 S. R. Gano K2-12 D. J. Trimble H0-40 W. J. Gray P7-27 J. H. Wicks, Jr. X3-74 G. S. Klinger P7-22 SNF Project Files D. K. Kreid K7-80 J. M. Latkovich K9-44 S. Fluor Daniel Hanford S. C. Marschman (10) P7-27 B. M. Oliver P7-22 E. W. Gerber R3-11 T. M. Orlando K8-88		G. D. Trenchard	S7-41		E. R. Cramer	H0-34	
Hanford Inc. C. R. Miska R3-86 J. P. Sloughter H5-49 R. B. Baker H0-40 D. W. Bergmann X3-79 SGN Eurisys Services Corp S. A. Chastain H0-40 D. R. Duncan R3-86 A. L. Pajunen R3-86 J. R. Frederickson R3-86 L. H. Goldmann R3-86 2 Technical Advisory Group S. L. Hecht H0-40 J. J. Jernberg X3-72 J. C. Devine R3-11 L. A. Lawrence (5) H0-40 R. F. Williams R3-11 B. J. Makenas H0-40 R. P. Omberg H0-40 32 Pacific Northwest National Laboratory R. W. Rasmussen X3-85 A. M. Segrest R3-11 J. Abrefah (5) P7-27 J. A. Swenson R3-11 J. P. Cowin K8-88 C. A. Thompson R3-86 S. R. Gano K2-12 D. J. Trimble H0-40 W. J. Gray P7-27 D. J. Watson X3-79 B. D. Hanson P7-27 J. H. Wicks, Jr. X3-74 G. S. Klinger P7-22 SNF Project Files D. K. Kreid K7-80 J. M. Latkovich K9-44 3 Fluor Daniel Hanford S. C. Marschman (10) P7-27 B. M. Oliver P7-22 E. W. Gerber R3-11 T. M. Orlando K8-88					T. A. Flament	H5-25	
R. B. Baker H0-40 D. W. Bergmann X3-79 S. A. Chastain H0-40 D. R. Duncan R3-86 J. R. Frederickson R3-86 L. H. Goldmann R3-86 L. H. Goldmann R3-86 S. L. Hecht HO-40 J. J. Jernberg X3-72 L. A. Lawrence (5) H0-40 R. P. Omberg H0-40 R. P. Omberg H0-40 R. W. Rasmussen X3-85 A. M. Segrest R3-11 J. A. Swenson R3-11 J. A. Swenson R3-11 J. A. Swenson R3-86 C. A. Thompson R3-86 C. A. Thompson R3-86 C. A. Thompson R3-86 S. R. Gano K2-12 D. J. Trimble H0-40 W. J. Gray P7-27 J. H. Wicks, Jr. X3-74 G. S. Klinger P7-22 SNF Project Files Fluor Daniel Hanford FR. W. Gerber R3-11 J. P. Cowin K8-88 Fluor Daniel Hanford Fractional H5-49 SGN Eurisys Services Corp R3-86 A. L. Pajunen R3-86 L. P. Opjunen R3-86 L. P. Opjunen R3-86 R3-11 J. C. Devine R3-11 J. C. Devine R3-11 J. A. F. Williams R3-11 J. Abrefah (5) P7-27 J. A. Swenson R3-11 J. Abrefah (5) P7-27 J. A. Swenson R3-11 J. P. Cowin K8-88 C. A. Thompson R3-86 S. R. Gano K2-12 D. J. Trimble H0-40 W. J. Gray P7-27 D. J. Watson X3-79 B. D. Hanson P7-27 J. H. Wicks, Jr. X3-74 G. S. Klinger P7-22 SNF Project Files J. M. Latkovich K9-44 S. C. Marschman (10) P7-27 B. M. Oliver P7-22 E. W. Gerber	23	Duke Engineering and Services	<u>.</u>		J. J. Irwin	R3-86	
R. B. Baker D. W. Bergmann X3-79 S. A. Chastain H0-40 D. R. Duncan R3-86 J. R. Frederickson R3-86 L. H. Goldmann R3-86 R3-11 L. A. Lawrence (5) R0-40 R. F. Williams R3-11 R3-11 R3-11 R3-11 R3-11 R3-11 R4-11 R3-11 R3-11 R3-11 R3-11 R4-11 R3-11 R3-11 R3-11 R3-11 R4-11 R3-11 R3-		Hanford Inc.			C. R. Miska	R3-86	
D. W. Bergmann S. A. Chastain H0-40 D. R. Duncan R3-86 J. R. Frederickson R3-86 L. H. Goldmann R3-86 S. L. Hecht J. J. Jernberg X3-72 L. A. Lawrence (5) B. J. Makenas H0-40 R. P. Omberg R. W. Rasmussen X3-85 A. M. Segrest R3-11 J. A. Swenson R3-86 C. A. Thompson R3-86 R3-86 R3-11 D. J. Trimble H0-40 W. J. Gray D. J. Trimble H0-40 D. J. Watson X3-79 J. H. Wicks, Jr. SNF Project Files Fluor Daniel Hanford FRIGHT A. Lawrence (10) FRIGHT					J. P. Sloughter	H5-49	
S. A. Chastain D. R. Duncan R3-86 J. R. Frederickson R3-86 L. H. Goldmann R3-86 R3-11 L. A. Lawrence (5) R0-40 R. F. Williams R3-11 R3-11		R. B. Baker	H0-40				
D. R. Duncan R3-86 J. R. Frederickson R3-86 L. H. Goldmann R3-86 L. H. Goldmann R3-86 S. L. Hecht HO-40 J. J. Jernberg X3-72 J. C. Devine R3-11 L. A. Lawrence (5) H0-40 R. P. Omberg H0-40 R. W. Rasmussen X3-85 A. M. Segrest R3-11 J. A. Swenson R3-11 J. A. Swenson R3-11 J. P. Cowin K8-88 C. A. Thompson R3-86 C. A. Thompson R3-86 S. R. Gano K2-12 D. J. Trimble H0-40 W. J. Gray P7-27 J. H. Wicks, Jr. X3-74 G. S. Klinger P7-22 SNF Project Files D. K. Kreid K7-80 J. M. Latkovich K9-44 S. C. Marschman (10) P7-27 B. M. Oliver P7-22 E. W. Gerber R3-11 T. M. Orlando K8-88		D. W. Bergmann	X3-79		SGN Eurisys Services Corp		
J. R. Frederickson R3-86 L. H. Goldmann R3-11 L. A. Lawrence (5) H0-40 R. F. Williams R3-11 R. F. Willi		S. A. Chastain	H0-40				
L. H. Goldmann S. L. Hecht HO-40 J. J. Jernberg X3-72 J. C. Devine R3-11 L. A. Lawrence (5) H0-40 R. F. Williams R3-11 B. J. Makenas H0-40 R. P. Omberg H0-40 R. W. Rasmussen X3-85 A. M. Segrest R3-11 J. Abrefah (5) P7-27 J. A. Swenson R3-11 J. P. Cowin K8-88 C. A. Thompson R3-86 S. R. Gano K2-12 D. J. Trimble H0-40 W. J. Gray P7-27 J. H. Wicks, Jr. X3-79 J. H. Wicks, Jr. SNF Project Files D. K. Kreid J. M. Latkovich K9-44 S. Fluor Daniel Hanford E. W. Gerber R3-11 R3-86 R3-11 R3-86 R3-86 S. R. Gano R3-12 R4-86 S. R. Gano R4-12 R5-12 R5-12 R5-13 R5-14 R5-14 R5-15 R5-16 R5-16 R5-16 R5-17 R5-17 R5-18 R5-11 R5-18 R5-11 R5-18 R5-11 R5-18 R5-11 R5-18 R5-11 R		D. R. Duncan	R3-86		A. L. Pajunen	R3-86	
S. L. Hecht HO-40 J. J. Jernberg X3-72 J. C. Devine R3-11 L. A. Lawrence (5) H0-40 R. F. Williams R3-11 B. J. Makenas H0-40 R. F. Williams R3-11 R. P. Omberg H0-40 32 Pacific Northwest National Laboratory R. W. Rasmussen X3-85 X3-85 A. M. Segrest R3-11 J. Abrefah (5) P7-27 J. A. Swenson R3-11 J. P. Cowin K8-88 C. A. Thompson R3-86 S. R. Gano K2-12 D. J. Trimble H0-40 W. J. Gray P7-27 D. J. Watson X3-79 B. D. Hanson P7-27 J. H. Wicks, Jr. X3-74 G. S. Klinger P7-22 SNF Project Files D. K. Kreid K7-80 J. M. Latkovich K9-44 3 Fluor Daniel Hanford S. C. Marschman (10) P7-27 B. M. Oliver P7-22 E. W. Gerber R3-11 T. M. Orlando K8-88		J. R. Frederickson	R3-86				
J. J. Jernberg X3-72 J. C. Devine R3-11 L. A. Lawrence (5) H0-40 R. F. Williams R3-11 B. J. Makenas H0-40 32 Pacific Northwest National Laboratory R. P. Omberg H0-40 32 Pacific Northwest National Laboratory R. W. Rasmussen X3-85 A. M. Segrest R3-11 J. Abrefah (5) P7-27 J. A. Swenson R3-11 J. P. Cowin K8-88 C. A. Thompson R3-86 S. R. Gano K2-12 D. J. Trimble H0-40 W. J. Gray P7-27 D. J. Watson X3-79 B. D. Hanson P7-27 J. H. Wicks, Jr. X3-74 G. S. Klinger P7-22 SNF Project Files D. K. Kreid K7-80 J. M. Latkovich K9-44 3 Fluor Daniel Hanford S. C. Marschman (10) P7-27 B. M. Oliver P7-22 E. W. Gerber R3-11 T. M. Orlando K8-88		L. H. Goldmann	R3-86	2	Technical Advisory Group		
L. A. Lawrence (5) H0-40 R. F. Williams R3-11 B. J. Makenas H0-40 R. P. Omberg H0-40 32 Pacific Northwest National Laboratory R. W. Rasmussen X3-85 A. M. Segrest R3-11 J. Abrefah (5) P7-27 J. A. Swenson R3-11 J. P. Cowin K8-88 C. A. Thompson R3-86 S. R. Gano K2-12 D. J. Trimble H0-40 W. J. Gray P7-27 D. J. Watson X3-79 B. D. Hanson P7-27 J. H. Wicks, Jr. X3-74 G. S. Klinger P7-22 SNF Project Files D. K. Kreid K7-80 J. M. Latkovich K9-44 Fluor Daniel Hanford S. C. Marschman (10) P7-27 B. M. Oliver P7-22 E. W. Gerber R3-11 T. M. Orlando K8-88		S. L. Hecht	HO-40				
B. J. Makenas H0-40 R. P. Omberg H0-40 R. W. Rasmussen X3-85 A. M. Segrest R3-11 J. A. Swenson R3-11 C. A. Thompson R3-86 D. J. Trimble H0-40 W. J. Gray P7-27 D. J. Watson X3-79 J. H. Wicks, Jr. X3-74 SNF Project Files D. K. Kreid K7-80 J. M. Latkovich K9-44 Fluor Daniel Hanford S. C. Marschman (10) P7-27 B. M. Oliver P7-22 E. W. Gerber R3-11 T. M. Orlando K8-88		J. J. Jernberg	X3-72		J. C. Devine	R3-11	
R. P. Omberg H0-40 32 Pacific Northwest National Laboratory R. W. Rasmussen X3-85 A. M. Segrest R3-11 J. Abrefah (5) P7-27 J. A. Swenson R3-11 J. P. Cowin K8-88 C. A. Thompson R3-86 S. R. Gano K2-12 D. J. Trimble H0-40 W. J. Gray P7-27 D. J. Watson X3-79 B. D. Hanson P7-27 J. H. Wicks, Jr. X3-74 G. S. Klinger P7-22 SNF Project Files D. K. Kreid K7-80 J. M. Latkovich K9-44 S. C. Marschman (10) P7-27 B. M. Oliver P7-22 E. W. Gerber R3-11 T. M. Orlando K8-88		L. A. Lawrence (5)	H0-40		R. F. Williams	R3-11	
R. W. Rasmussen X3-85 A. M. Segrest R3-11 J. Abrefah (5) P7-27 J. A. Swenson R3-11 J. P. Cowin K8-88 C. A. Thompson R3-86 S. R. Gano K2-12 D. J. Trimble H0-40 W. J. Gray P7-27 D. J. Watson X3-79 B. D. Hanson P7-27 J. H. Wicks, Jr. X3-74 G. S. Klinger P7-22 SNF Project Files D. K. Kreid K7-80 J. M. Latkovich K9-44 3 Fluor Daniel Hanford S. C. Marschman (10) P7-27 B. M. Oliver P7-22 E. W. Gerber R3-11 T. M. Orlando K8-88		B. J. Makenas	H0-40				
A. M. Segrest R3-11 J. Abrefah (5) P7-27 J. A. Swenson R3-11 J. P. Cowin K8-88 C. A. Thompson R3-86 S. R. Gano K2-12 D. J. Trimble H0-40 W. J. Gray P7-27 D. J. Watson X3-79 B. D. Hanson P7-27 J. H. Wicks, Jr. X3-74 G. S. Klinger P7-22 SNF Project Files D. K. Kreid K7-80 J. M. Latkovich K9-44 Fluor Daniel Hanford S. C. Marschman (10) P7-27 B. M. Oliver P7-22 E. W. Gerber R3-11 T. M. Orlando K8-88		R. P. Omberg	H0-40	32	Pacific Northwest National Lal	ooratory	
J. A. Swenson R3-11 J. P. Cowin K8-88 C. A. Thompson R3-86 S. R. Gano K2-12 D. J. Trimble H0-40 W. J. Gray P7-27 D. J. Watson X3-79 B. D. Hanson P7-27 J. H. Wicks, Jr. X3-74 G. S. Klinger P7-22 SNF Project Files D. K. Kreid K7-80 J. M. Latkovich K9-44 3 Fluor Daniel Hanford S. C. Marschman (10) P7-27 B. M. Oliver P7-22 E. W. Gerber R3-11 T. M. Orlando K8-88		R. W. Rasmussen	X3-85				
C. A. Thompson R3-86 S. R. Gano K2-12 D. J. Trimble H0-40 W. J. Gray P7-27 D. J. Watson X3-79 B. D. Hanson P7-27 J. H. Wicks, Jr. X3-74 G. S. Klinger P7-22 SNF Project Files D. K. Kreid K7-80 J. M. Latkovich K9-44 3 Fluor Daniel Hanford S. C. Marschman (10) P7-27 B. M. Oliver P7-22 E. W. Gerber R3-11 T. M. Orlando K8-88		A. M. Segrest	R3-11		J. Abrefah (5)	P7-27	
D. J. Trimble H0-40 W. J. Gray P7-27 D. J. Watson X3-79 B. D. Hanson P7-27 J. H. Wicks, Jr. X3-74 G. S. Klinger P7-22 SNF Project Files D. K. Kreid K7-80 J. M. Latkovich K9-44 Fluor Daniel Hanford S. C. Marschman (10) P7-27 B. M. Oliver P7-22 E. W. Gerber R3-11 T. M. Orlando K8-88		J. A. Swenson	R3-11		J. P. Cowin	K8-88	
D. J. Watson X3-79 B. D. Hanson P7-27 J. H. Wicks, Jr. X3-74 G. S. Klinger P7-22 SNF Project Files D. K. Kreid K7-80 J. M. Latkovich K9-44 3 Fluor Daniel Hanford S. C. Marschman (10) P7-27 B. M. Oliver P7-22 E. W. Gerber R3-11 T. M. Orlando K8-88		C. A. Thompson	R3-86		S. R. Gano	K2-12	
J. H. Wicks, Jr. X3-74 G. S. Klinger P7-22 SNF Project Files D. K. Kreid K7-80 J. M. Latkovich K9-44 S. C. Marschman (10) P7-27 B. M. Oliver P7-22 E. W. Gerber R3-11 T. M. Orlando K8-88		D. J. Trimble	H0-40		W. J. Gray	P7-27	
SNF Project Files D. K. Kreid K7-80		D. J. Watson	X3-79		B. D. Hanson	P7-27	
J. M. Latkovich K9-44 3 Fluor Daniel Hanford S. C. Marschman (10) P7-27 B. M. Oliver P7-22 E. W. Gerber R3-11 T. M. Orlando K8-88		J. H. Wicks, Jr.	X3-74		G. S. Klinger	P7-22	
Fluor Daniel Hanford S. C. Marschman (10) P7-27 B. M. Oliver P7-22 E. W. Gerber R3-11 T. M. Orlando K8-88		SNF Project Files			D. K. Kreid	K7-80	
B. M. Oliver P7-22 E. W. Gerber R3-11 T. M. Orlando K8-88					J. M. Latkovich	K9-44	
E. W. Gerber R3-11 T. M. Orlando K8-88	3	Fluor Daniel Hanford			S. C. Marschman (10)	P7-27	
					B. M. Oliver	P7-22	
D. A. Smith T4-13 J. C. Wiborg K7-74		E. W. Gerber	R3-11		T. M. Orlando	K8-88	
		D. A. Smith	T4-13		J. C. Wiborg	K7-74	
M. J. Wiemers R3-11 Information Release (7)	٠	M. J. Wiemers	R3-11		Information Release (7)		